Airplane Measurements of Planetary Boundary Layer Structure

D. H. LENSCHOW

National Center for Atmospheric Research,[1] Boulder, Colo.

(Manuscript received 17 April 1970, in revised form 25 August 1970)

ABSTRACT

Measurements of air velocity and temperature from an airplane in the planetary boundary layer with strong surface heating are used to calculate vertical heat, momentum and energy fluxes, as well as spectral densities and probability distributions of velocity and temperature. Airplane traverses parallel to the wind are compared to crosswind traverses and a definite elongation of the heat transporting eddies, or thermals, parallel to the wind is observed. The terms in the turbulent kinetic energy balance equation (with the exception of the pressure fluctuation term) and the temperature variance balance equation are estimated. The turbulent kinetic energy dissipation is almost constant with height between the lowest flight level of 100 m above the surface, and the highest flight level of 1000 m, which is just below the top of the boundary layer, while the generation term due to the buoyancy force decreases and the divergence of the vertical transport of kinetic energy increases with height to maintain an approximate balance. The temperature variance dissipation decreases rapidly with height and the generation of temperature variance and the divergence of the vertical transport of temperature variance become small above 100 m.

1. Introduction

This paper presents the results of a series of measurements from an aircraft over relatively flat and uniform terrain in eastern Colorado during a period of large upward heat flux. The variables measured were sufficient to calculate fluctuations in air velocity along all three airplane axes, mean wind, temperature, pressure altitude and humidity. The general method of measuring vertical velocity fluctuations and temperature is similar to that described by Warner and Telford (1962), who made measurements under conditions similar to those of the present study. Myrup (1969) made airborne turbulence measurements under unstable conditions and also attempted to evaluate the turbulent kinetic energy equation, as is done here, but he did not have measurements of the vertical transport of kinetic energy.

Measurements were taken at four different altitudes within the planetary boundary layer at aircraft headings perpendicular and parallel to the mean wind. The heat transporting eddies, or thermals, were elongated in the direction of the wind. Various other investigators have noted such asymmetric structure in the boundary layer. Kuettner (1959) described in detail observations of convective streets, especially cloud streets, and discussed the conditions necessary for their occurrence. Hardy and Ottersten (1969) observed radar returns indicating that cells or thermals are often organized in streets parallel to the wind.

[1] The National Center for Atmospheric Research is sponsored by the National Science Foundation.

2. Description of sensors and measurements

The sensors used for this series of measurements can be divided into two groups—those for air measurements and those for determining the position and orientation of the airplane. The outputs of the instruments were recorded digitally on magnetic tape. Variables used for calculating the high-frequency variation of temperature and velocity were recorded 32 times per second and later averaged over four samples, whereas the remaining measurements were recorded 8 times per second.

The air measurement sensors were located on a boom $\sim$1.5 m in front of the nose of the aircraft. The attack and sideslip angles of the airplane were measured with "fixed" vane sensors, which are constrained from rotating and measure the force exerted on the vane by the airstream perpendicular to the surface of the vane. The angle of the airstream with respect to the vane is given by

$$\alpha = CA(F/q), \tag{1}$$

where q is the dynamic pressure measured with a pitot-static tube at the tip of the boom, A the vane area ($=50$ cm^2), F the force on the vane, and C an empirical constant measured in a wind tunnel to be $\sim$2.8 for the vanes used here, valid for angles $\alpha \lesssim 0.2$ rad. The force is measured by means of strain gages mounted on the beam that supports the vane, which is very nearly critically damped by a viscous silicone fluid between two closely-spaced parallel plates that move with respect to each other when the force on the vane changes. The natural frequency of the vane is $\sim$150 Hz. The dynamic pressure is also used, along with temperature

and altitude, to calculate the true airspeed of the airplane. Two probes are used for measuring temperature, one a platinum resistance wire shielded from the direct airstream for measuring mean temperature, and the other a 25 μ diameter tungsten wire mounted directly in the airstream for measuring temperature fluctuations with a time constant of $\sim$0.01 sec at an airspeed of 80 m sec^{-1}.

A Doppler radar is used to measure the ground speed and drift angle of the airplane, from which the horizontal velocity of the airplane with respect to the earth can be determined. The vertical velocity of the airplane is obtained from the integrated output of an accelerometer mounted on a gyroscopically-stabilized platform. This velocity is combined with the pitch angle (the angle between the stabilized platform and the airplane), the angle of attack, and the true airspeed to obtain the vertical air velocity. The method used to calculate the three velocity components from these sensor outputs is given in the Appendix.

The mean and trend are removed from the temperature and the horizontal air velocity components, and a quadratic curve is removed from the vertical air velocity by a least-squares fit. The longitudinal and lateral velocity components are also transformed to make them correspond more closely to the conventional meteorological coordinate system. The x axis, which defines the u component, is in the direction of the mean wind; the z axis which defines the w component, is pointing up; while the y axis, which defines the v component, is perpendicular to x and z in a right-handed coordinate system.

Measurements were made on 25 April 1968 over a flat treeless area of eastern Colorado where the slope of the terrain is about 0.2% toward the NNE, and variations in elevation excluding the mean slope are less than 20 m. Two sets of horizontal runs, parallel and perpendicular to the mean wind within 10°, and 15–20 km long, were made at heights of 100, 200, 450 and 1000 m above the surface from 0942–1100 MST. Because the runs were made at constant pressure altitudes, the heights above the surface are the estimated average heights. Two vertical soundings of temperature taken by the airplane between and after the two sets of runs are plotted in Fig. 1, along with the mean wind measured at each level. The upward heat flux at 100 m above the surface, measured by the eddy correlation technique, was 25 mW cm^{-2}, or about 17% of the solar constant. A cold front had passed through this region several hours earlier, and the ground may not yet have responded completely to the colder air. Scattered stratocumulus clouds existed just above 1000 m above the surface.

3. Time series and spectral analysis

In this section the time series records of temperature and air velocity at the four flight levels are analyzed and

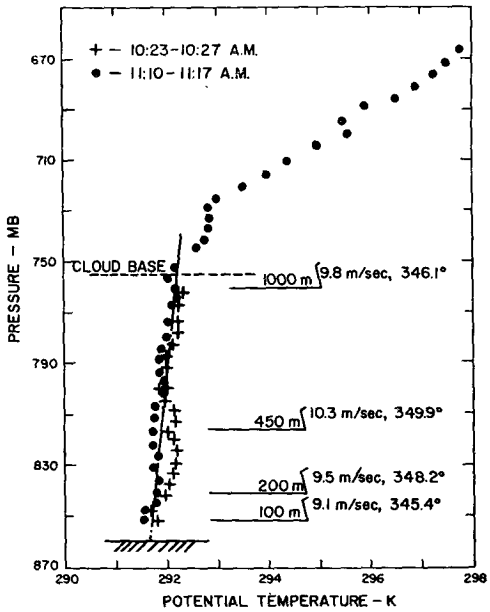

FIG. 1. The mean state of the atmosphere during the measurement runs on 25 April 1968.

discussed. The space-lagged correlation coefficient of vertical velocity and temperature is used to quantify estimates of the sizes of the heat transporting eddies. The number of zero crossings, the cumulative probability distributions, and spectral densities are also computed for temperature and velocity at several flight levels. An evaluation of the accuracy of the heat flux measurements is obtained from a computation of the

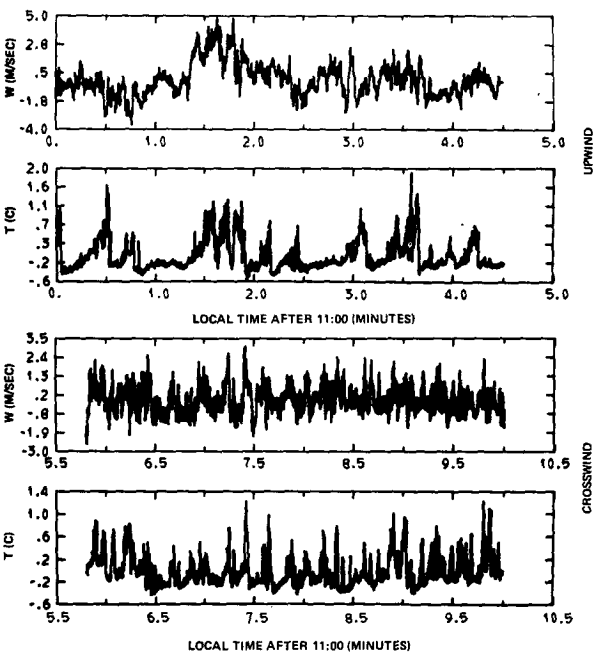

FIG. 2. Air temperature and vertical velocity at 100 m above the surface for both upwind and crosswind airplane traverses.

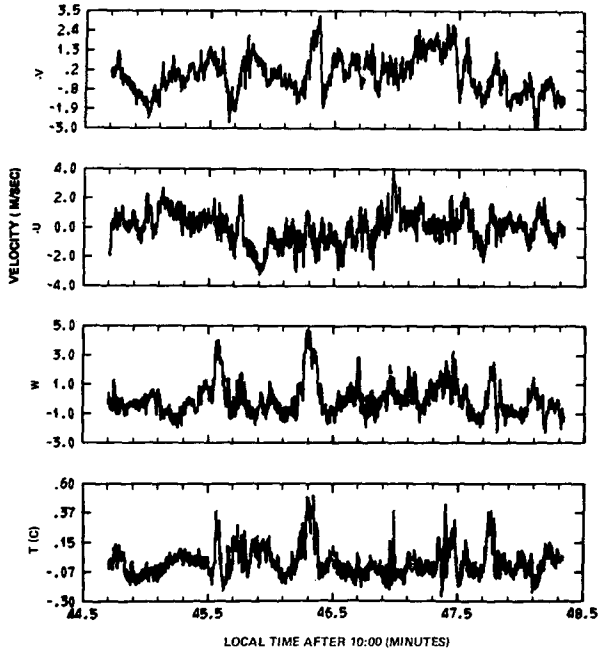

FIG. 3. Air temperature and velocity at 450 m above the surface with the airplane flying perpendicular to the wind. The direction of the wind is from right to left across the front of the aircraft, and the directions of the velocity components are defined in the text. The $-v$ component is the measured longitudinal velocity, and the $-u$ component the measured lateral velocity.

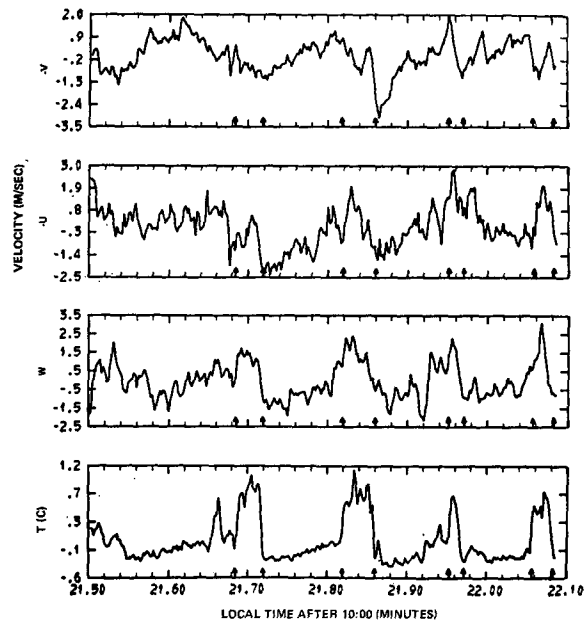

FIG. 4. An expanded section of a time series plot at 100 m above the surface with the airplane flying in the same direction as in Fig. 3. The arrows along the abscissa delineate the edges of thermals.

significant terms in the equation of the local rate of change of temperature with time.

A definite horizontal asymmetry exists in the velocity and temperature fields. Fig. 2 indicates that when flying crosswind the number of penetrations of heat-transporting eddies, or thermals, is larger and the size of these thermals is smaller than when flying parallel to the wind. Fig. 3 shows that at 450 m the thermals are fewer but of a slightly larger size than at 100 m. Another noteworthy feature is the occurrence of a maximum change in v at the edges of the thermals with the aircraft flying in a crosswind direction. If a thermal were entraining a significant amount of environmental air along the edges parallel to the wind, v should first decrease below the mean then increase above the mean when flying in the negative y direction, which was the direction flown for the measurements shown in Figs. 3 and 4. Of the four distinct thermals in Fig. 4, two coincide with a relatively large decrease in v across the thermal. The other two coincide with changes in u, which might be expected if the airplane penetrated the edge of a thermal. No indication of rotation of the thermals has been observed, which is in agreement with the observations reported by Kaimal and Businger (1970) from a 32 m tower. If the thermals were rotating, the component of the velocity fluctuation at right angles to the flight path (the u component in Figs. 3 and 4) would change from a large positive or negative value on one side of the thermals to a large value of opposite sign on the other.

Fig. 4 also demonstrates, as Warner and Telford (1963) have observed, that temperature is the best indicator of a thermal because of the large difference in temperature between the inside and outside of a thermal, compared with the relatively small temperature variance outside a thermal. The difference in vertical velocity averaged inside and outside a thermal is similar in magnitude, in many cases, to the level of velocity fluctuations outside a thermal. Since the mean airplane velocity for these flights is $\sim$80 m sec^{-1}, the thermals shown in Fig. 4 are $\sim$200 m across.

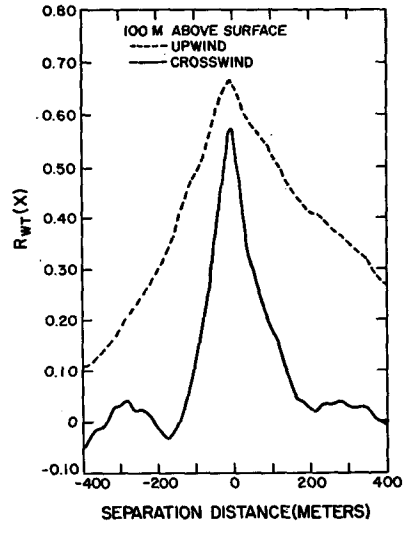

FIG. 5. A comparison of the space-lagged correlation coefficient of vertical velocity and temperature for upwind and crosswind airplane traverses.

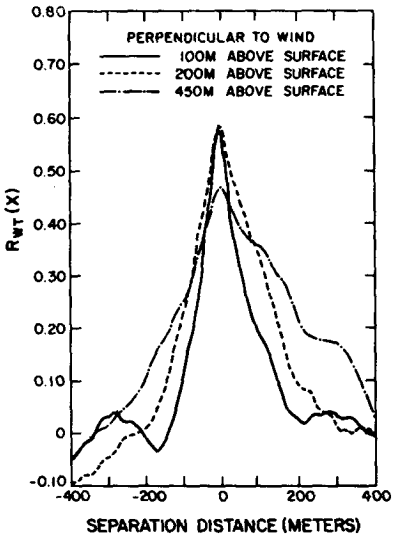

FIG. 6. The space-lagged correlation coefficient of vertical velocity and temperature as a function of height above the ground.

Another estimate of the size of the thermals can be obtained by computing a space-lagged correlation coefficient of vertical velocity and temperature, i.e.,

$$R_{wT}(x)=\frac{\overline{w(r+x)T(r)}}{\sigma_w\sigma_T}, \qquad (2)$$

where the bar indicates a line average, and σ_w and σ_T are the standard deviations of vertical velocity and temperature, respectively. Fig. 5 shows that at 100 m above the surface the lagged heat flux drops to zero at a lag of about 200 m for the crosswind run which corresponds well to the sizes of the thermals estimated from the time traces. The observed scale length of the thermals on the upwind run is greater than 400 m. The curves have the triangular shape characteristic of a "top hat" thermal; that is, the space-lagged correlation coefficient curve for rectangular temperature and vertical velocity pulses is a triangle.

The size of the thermals also changes with height; the thermals at 450 m are approximately double the size of those at 100 m above the surface (Fig. 6). These dimensions can be compared with the dimensions observed in the radar investigations of Hardy and Ottersten (1969). These investigators obtained dimensions of 1–3 km for what they term Type I cells, which seemed to originate several hundred meters above the surface. It would appear that the airplane was penetrating the source of the larger cells which were observed on the radar to extend through the top of the planetary boundary layer. However, a 12-min sample from the output of a vertically-pointed radar (*loc. cit.*) suggests a dimension of 500–700 m for thermals that extend up to about 1 km above the surface. The radar also has shown that the cells are organized in streets parallel to the wind if the surface wind is "not light."

Other investigators have shown that the necessary conditions for the development of convective streets were present for the flight described here. Woodcock (1942) noted that differences in the soaring techniques of sea gulls depended on the wind speed and temperature difference between water and air. At wind speeds of 7–13 m sec^{-1} and at water temperatures at least 4C higher than the air temperature, sea gulls soar straight to windward. At wind speeds <7 m sec^{-1} they soar in circular patterns. Kuettner (1959) observed that most extratropical cloud streets occur in vigorous outbreaks of polar air.

The number of zero crossings of the vertical velocity and temperature in Figs. 7 and 8 also gives a quantitative indication of the difference between upwind and crosswind flights. The ordinate is the number of times the variable intersects the value given by the abscissa, with increments of 0.015C and 0.1 m sec^{-1} for air temperature and vertical velocity, respectively. At 100 m above the surface, the values of vertical velocity between 0 and 1.5 m sec^{-1} have at least 50% more zero crossings when flying crosswind than upwind. The temperature trace between -0.1 and 1.0C has a similar

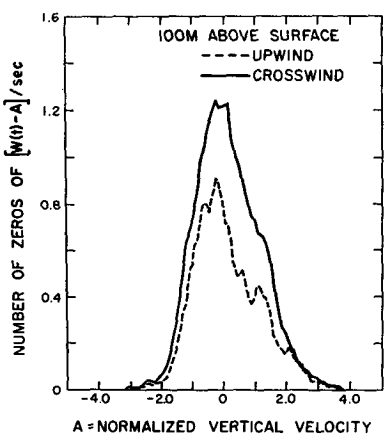

FIG. 7. Number of times the vertical velocity, normalized by σ_w, intersects the value of A.

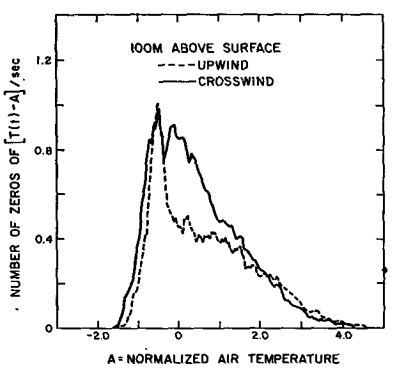

FIG. 8. Number of times the air temperature, normalized by σ_T, intersects the value of A.

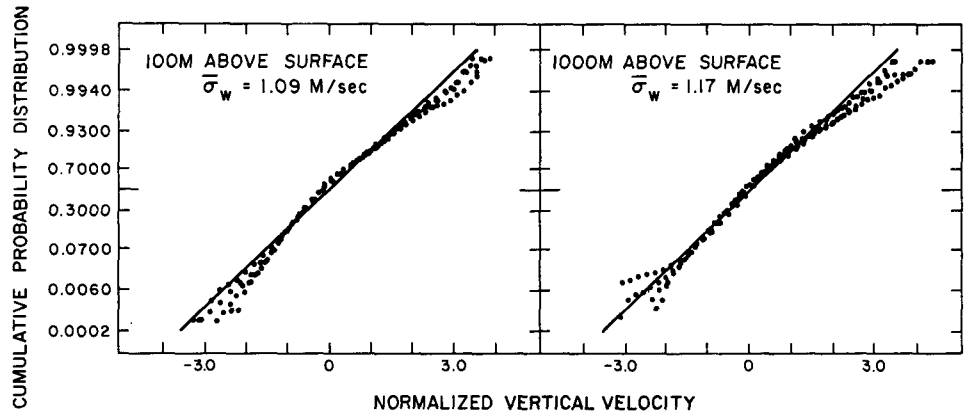

FIG. 9. Cumulative probability distribution for normalized vertical velocity averaged over all the airplane traverses at 100 and 1000 m above the surface. The straight line is a normal distribution.

behavior. The temperature also has an obviously more skewed probability distribution than the vertical velocity. The cumulative probability distributions for temperature and vertical velocity at 100 and 1000 m above the surface, plotted in Figs. 9 and 10, indicate that the skewness is greater at 100 than at 1000 m. A normal distribution in these figures is represented by a straight line. The temperature distribution can be approximated by two straight lines, the lower part being characteristic of fluctuations of temperature outside the thermals and the upper part characteristic of the inside of the thermals. This indicates that the temperature fluctuations inside a thermal are 3–4 times larger than those outside, and that a separate normal distribution fits each region reasonably well.

The spectral densities of vertical and longitudinal velocity and temperature at 100 m are plotted in Figs. 11–13. The data were averaged over four points before computing the spectral densities. The frequency response of a four-term mean with a sample interval in the original data of 1/32 sec is approximately $(8/\pi f) \times \sin(\pi f/8)$ (Holloway, 1958). When this function is squared and multiplied by the aliased spectral density (assuming a $-5/3$ spectral density slope), the effect of aliasing is very nearly cancelled. The spectral density estimates are the average of 5 Fourier modes for wavenumbers $\lesssim 15$ rad km^{-1} and about 25 Fourier modes for wavenumbers >15 rad km^{-1}, with smoothing weights of 0.25, 0.50 and 0.25. Furthermore, the measurement error increases as the wavenumber decreases, so that the spectral density estimates at low wavenumbers are not very significant. The curves do show, however, that at low wavenumbers the spectral densities measured parallel to the wind are larger than those measured perpendicular to the wind. The slopes of the spectral densities do not appear to depart significantly from $-5/3$. It should be remembered, however, that at most only the last one and one-half decade of the spectra are in the inertial subrange.

Since heat is vertically transported in sharp-edged pulses of a relatively limited range of sizes, rather than in slowly-varying eddies (in space), the spectral density of heat flux contributed by the thermals covers several decades of wavenumbers. Therefore, from a measurement standpoint, the instrumentation system should be capable of measuring wavelengths of greater than 1 km and less than 10 m in order to accurately measure the structure of thermals of nominally 200 m diameter.

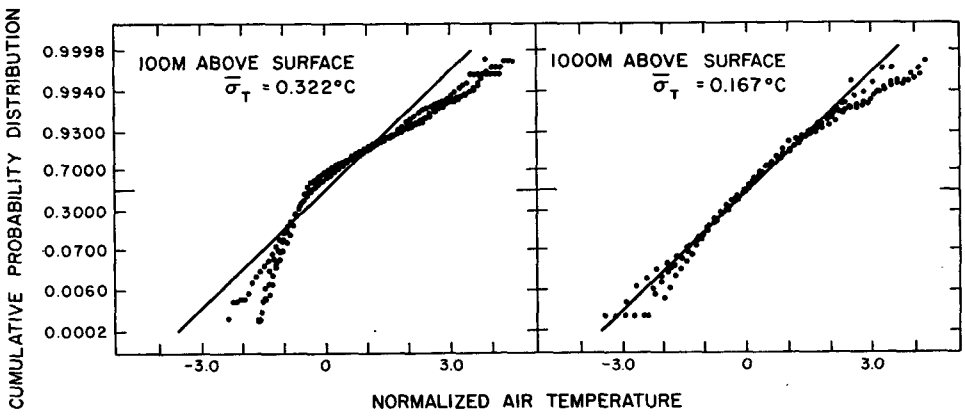

FIG. 10. Cumulative probability distribution for normalized air temperature averaged over all the airplane traverses at 100 and 1000 m above the surface. The straight line is a normal distribution.

Furthermore, the thermals present some sampling problems: the presence or absence of one thermal with a temperature excess of 0.5C and 300 m diameter over a 15-km flight path can change the mean temperature by 0.01C, the variance by $0.005C^2$, and the horizontal derivative of the temperature by 0.004C km^{-1}.

The local rate of change of temperature with time can be obtained from the equation of continuity and the equation of state for an ideal gas, as shown by Businger and Deardorff (1968) [neglecting $\partial/\partial y$ ( )], i.e.,

$$\bar{\rho}\frac{\partial\bar{T}}{\partial t}+\frac{\partial}{\partial t}(\overline{\rho'T'})=-\frac{\partial}{\partial x}[\overline{(\rho u)'T'}]-\frac{\partial}{\partial z}[\overline{(\rho w)'T'}]$$
$$-\bar{\rho}\bar{u}\frac{\partial\bar{T}}{\partial x}-\bar{\rho}\bar{w}\frac{\partial\bar{T}}{\partial z}+\frac{1}{C_p}\left(\frac{\overline{dP}}{dt}+\bar{\rho}\frac{\overline{dh}}{dt}\right), \quad (4)$$

where dh/dt is the rate of heating (by radiation) per unit mass. Measurements by Gossard (1960) and numerical experiments by Deardorff (1970) suggest that the pressure fluctuations, $|P'|$, are of the same order of magnitude as the turbulent kinetic energy, which was measured to be typically about 20 dyn cm^{-2}; thus, $P'/P\approx 2\times10^{-5}$. Since the temperature fluctuation term was typically 0.3C, or $T'/T\approx10^{-3}$, we can make the approximation

$$\rho'/\bar{\rho}\approx -T'/\bar{T}. \quad (5)$$

Substituting (5) into terms of (4), we obtain

$$\frac{\partial}{\partial t}(\overline{\rho'T'})\approx-\frac{\partial}{\partial t}\left(\frac{\bar{\rho}}{\bar{T}}\overline{T'^2}\right), \quad (6)$$

$$\frac{\partial}{\partial z}[\overline{(\rho w)'T'}]\approx\frac{\partial}{\partial z}\bar{\rho}\left(\overline{w'T'}-\frac{\bar{w}}{\bar{T}}\overline{T'^2}-\frac{\overline{w'T'^2}}{\bar{T}}\right), \quad (7)$$

$$\frac{\partial}{\partial x}[\overline{(\rho u)'T'}]\approx\frac{\partial}{\partial x}\bar{\rho}\left(\overline{u'T'}-\frac{\bar{u}}{\bar{T}}\overline{T'^2}-\frac{\overline{u'T'^2}}{\bar{T}}\right), \quad (8)$$

$$\bar{\rho}\bar{u}\frac{\partial\bar{T}}{\partial x}\approx\bar{\rho}\bar{u}\frac{\partial\bar{T}}{\partial x}+\left(\frac{\bar{\rho}}{\bar{T}}\right)\overline{u'T'}\frac{\partial\bar{T}}{\partial x}. \quad (9)$$

Typical measured values for the moment terms on the right side of the above equations are $\overline{w'T'}\approx20$ cm (°C) sec^{-1}, $\overline{T'^2}\approx0.1(°C)^2$ and $\overline{w'T'^2}\approx10$ cm $(°C)^2$ sec^{-1}. Thus, the only significant term in (6) and (7) is $\partial/\partial z[\bar{\rho}(\overline{w'T'})]$. The terms in parenthesis on the right side of (8) are similar in magnitude to the analogous terms in (7), but the horizontal length scale is about 20 times the vertical, so all the terms in (8), as well as the previously neglected y component terms, can be neglected. The first term in (9) is at least three orders of magnitude larger than the second. Introducing potential temperature and rewriting the fourth and fifth terms on the right side of (4), we have

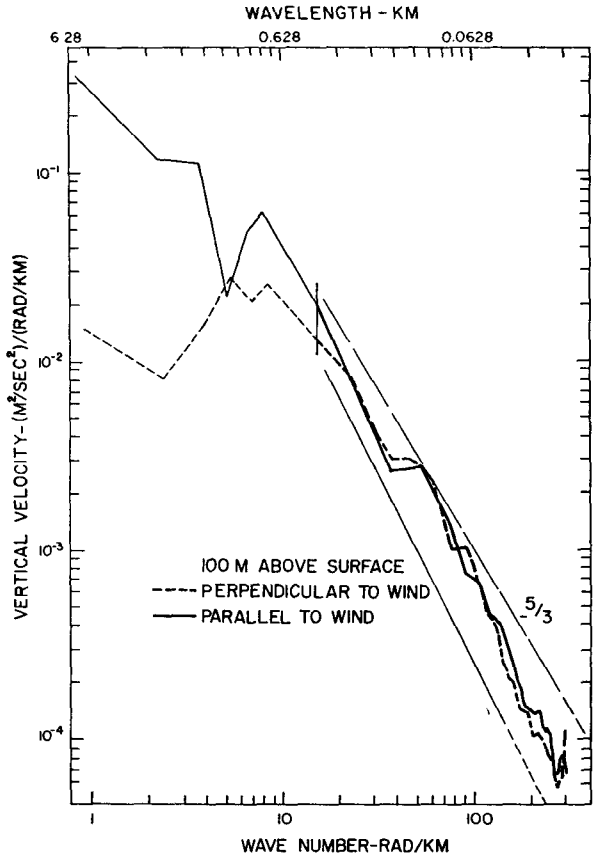

FIG. 11. Spectral density of vertical velocity. The individual spectral estimates to the right of the line at 15 rad km^{-1} are made up of about 25 Fourier modes and smoothed; the estimates to the left are the average of 5 Fourier modes.

$$-\overline{\rho w}(\bar{T}/\bar{\theta})\partial\bar{\theta}/\partial z+(1/C_p)\left(\frac{\overline{\partial P}}{\partial t}+\overline{u\partial P/\partial x}\right).$$

The lapse rate is very nearly neutral, and the wind direction is almost parallel to the local elevation contours, so the mean vertical mass flux times the lapse rate is considered negligible. The horizontal pressure gradient term, divided by the density, is less than 10^{-6}C sec^{-1}, and since the measurements were made on a constant pressure surface, these terms are also negligible. Using the results of Sasamori (1968), the radiational cooling is estimated to be 10^{-5}C sec^{-1}, which is about an order of magnitude less than the typical values of the remaining terms in (4), i.e.,

$$\frac{\partial\bar{T}}{\partial t}=-\bar{u}\frac{\partial\bar{T}}{\partial x}-\frac{\partial}{\partial z}(\overline{w'T'}). \quad (10)$$

These terms have been evaluated for the measurements from the airplane and the results are given in Fig. 14. Warner and Telford (1965) made a similar

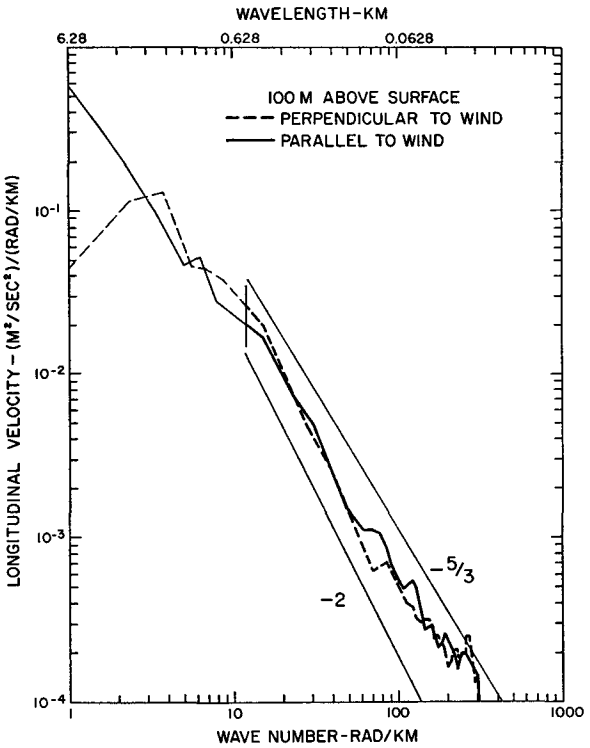

FIG. 12. Same as Fig. 11 except for longitudinal velocity.

analysis, except that their airplane was allowed to drift with the local mean wind so that the first term on the right of (10) was zero.

The term on the left side of (10) is obtained from the local change in temperature between each set of runs. The value of $\partial\bar{T}/\partial x$ is obtained from the runs parallel to the wind, and $\bar{u}$ and the flux divergence from both the parallel and crosswind runs. As indicated earlier, the presence or absence of one thermal can change $\partial\bar{T}/\partial x$ by 0.004C km^{-1}, which would change the first term on the right in Eq. (10) by 0.4×10^{-4}C sec^{-1}. For this reason, the horizontal temperature derivative was evaluated by eye rather than by a more objective technique such as a least-squares fit. If the equation is evaluated between each successive flight level, the flux divergence term appears to be too large in the lowest layer and too small in the highest level. Considering the boundary layer as a whole, the equation is balanced. Therefore, the temperature flux measured at 100 m appears to be consistent with the observed time rate of change of temperature and temperature advection. The residual in the equation for the 100–200 m layer can be removed if the measured vertical temperature flux at 200 m is assumed to be 14% too small. Similarly, if the measured flux at 450 m is assumed to be 34% too small, the flux divergence in the upper two layers approximately balances the other two terms in the equation. The co-spectral densities of vertical velocity and temperature at 100 m indicate that the amount of heat flux in the wavenumber interval 4.5–13.5 rad km^{-1} is ~2.6 times the heat flux in the interval 13.5–22.5 rad km^{-1}; at 200 m it is ~4.9 times as large. Using the empirical "universal" co-spectra formulation of Panofsky and Mares (1968), we obtain the values 3.3 at 100 m and 4.6 at 200 m. This expression was obtained from tower measurements in the surface layer and has not been tested above it. This result does show, however, that the heat flux at long wavelengths becomes increasingly important at higher levels above the ground. Since errors in the vertical velocity increase with time, the heat flux measurement is less accurate at higher levels and possibly part of the heat flux is beyond the longest measured wavelength. The rather large value of cold air advection which almost balances the flux divergence is apparently due to a recent cold front that passed through this area.

4. Variance balance equations

The turbulent kinetic energy balance equation is given by

$$\frac{\partial\overline{e'}}{\partial t}=\frac{g}{T}(\overline{w'T'})-\frac{\partial}{\partial z}[\overline{w'(e'+P'/\rho)}]+\frac{\bar{\tau}}{\rho}\cdot\frac{\partial\bar{v}}{\partial z}-\bar{u}\frac{\partial\overline{e'}}{\partial x}-\epsilon, \quad (11)$$

where $\overline{e'}$ is the kinetic energy, $\frac{1}{2}(\overline{u'^2}+\overline{v'^2}+\overline{w'^2})$, $\bar{\tau}$ the

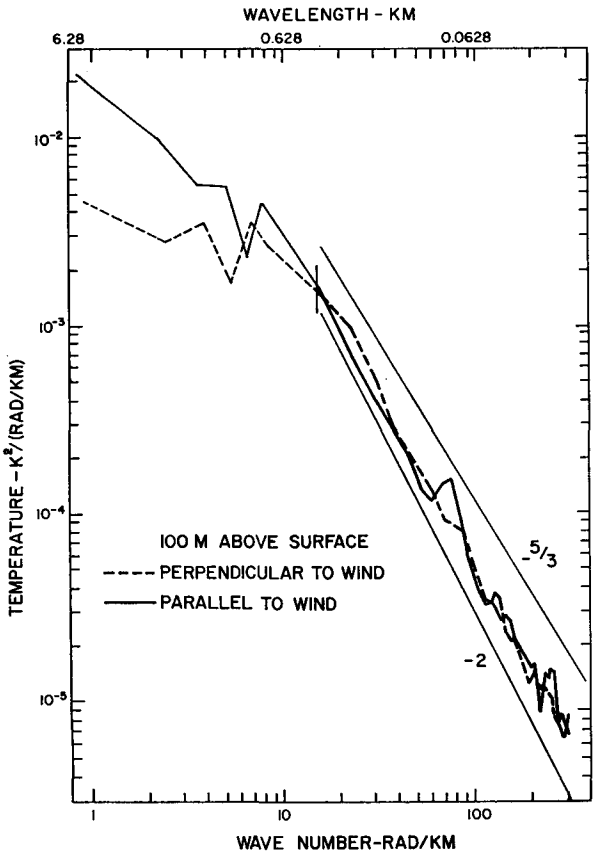

FIG. 13. Same as Fig. 11 except for spectral density of air temperature.

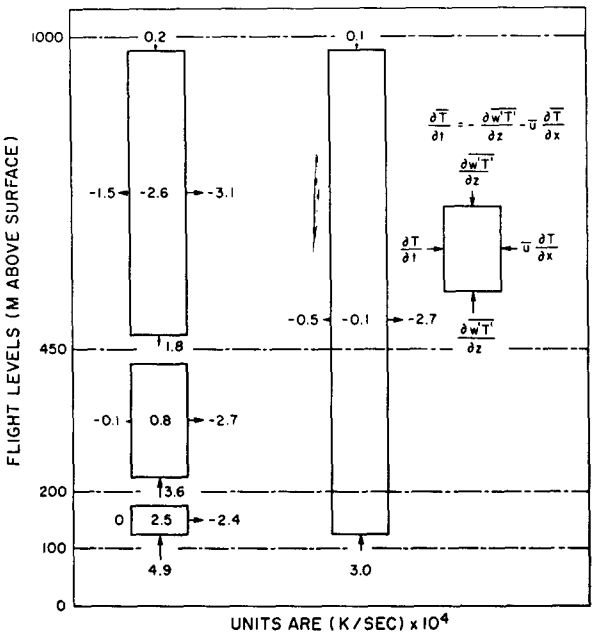

FIG. 14. Block diagram of the measured terms in the local air temperature budget. On the left, each layer between flight levels is considered individually; on the right, the boundary layer between 100 and 1000 m is considered as a whole.

stress, and ϵ the viscous energy dissipation. The pressure fluctuation term was not measured. Neglecting this term may introduce a significant error in the results since the pressure term, $|\overline{P'/\rho}|$, is of the same order of magnitude as $\overline{e'}$. The time rate of change of kinetic energy was measured to be almost two orders of magnitude and the horizontal advection of kinetic energy about one order of magnitude smaller than the other terms. Therefore, the equation that is evaluated is

$$\frac{g}{T}(\overline{w'T'})-\frac{\partial(\overline{w'e'})}{\partial z}+\frac{\bar{\tau}}{\rho}\cdot\frac{\partial\bar{v}}{\partial z}-\epsilon=R, \qquad (12)$$

where R is the residual necessary to balance the equation primarily because of the neglect of the pressure term. These terms are plotted in Fig. 15 as a function of height, using data from all four levels, averaged over both sets of runs. The vertical derivatives are evaluated between each flight level.

As was mentioned earlier, the vertical heat flux at the upper levels is probably underestimated. Thus, the actual buoyant energy production curve is probably closer to a straight line. This was to be expected if the lapse rate did not change with time and the horizontal advection of temperature were constant with height. Both of these assumptions appear to be valid for these measurements. Since the vertical termperature flux is underestimated, it is probable that the vertical kinetic energy flux is also underestimated at the upper levels. This underestimation means that the value of $[-\partial(\overline{w'e'})/\partial z]$ would be even smaller in the lower two layers and perhaps somewhat larger in the upper layer. The value of $(\overline{w'e'})$ is a maximum at 450 m. Estimates of $\bar{\tau}$ are obtained from

$$\tau/\rho=(\overline{u'w'})\mathbf{i}+(\overline{v'w'})\mathbf{j}. \qquad (13)$$

The stress is measured on flight legs parallel and perpendicular to the wind. These quantities are also probably underestimated, but the error is not so serious since we are not taking the vertical derivative and the term in the energy equation is considerably smaller than the other terms. The shear, $\partial\bar{v}/\partial z$, is obtained from the Doppler-measured airplane velocity and the true air speed at each level.

The energy dissipation is estimated from the spectral density of the longitudinal velocity, using the Kolmogoroff hypothesis for the inertial subrange, i.e.,

$$E(k)=\alpha\epsilon^{2/3}k^{-5/3}. \qquad (14)$$

The value $\alpha=0.47$, suggested by Panofsky and Pasquill (1963), was used in this equation with k in rad cm^{-1} and ϵ in cm^2 sec^{-3}.

We can conclude from Fig. 15 that the energy dissipation is almost constant with height. Also, the divergence of the vertical transport of kinetic energy, $\partial(\overline{w'e'})/\partial z$, increases with height so as to balance the buoyancy source term, $(g/T)(\overline{w'T'})$, which decreases with height to a slightly negative value at 1000 m. Furthermore, all the evaluated terms except the shear source term, $(\bar{\tau}/\rho)\cdot(\partial\bar{v}/\partial z)$, are generally of similar magnitude. The

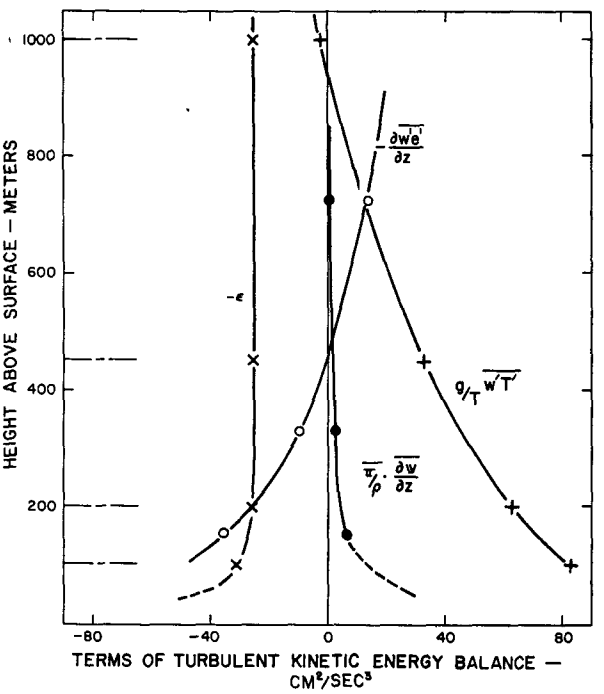

FIG. 15. Measured terms of the turbulent kinetic energy balance equation.

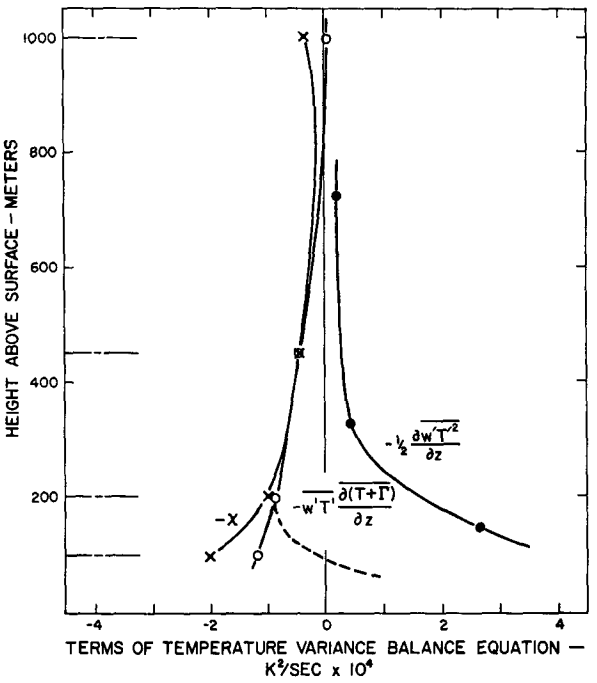

FIG. 16. Measured terms of the temperature variance balance equation.

shear source term is important only near the surface and perhaps in the vicinity of the inversion, where the shear again becomes significant.

The temperature variance balance equation is given by

$$\frac{1}{2}\frac{\partial\overline{T'^2}}{\partial t}=-\overline{(w'T')}\left(\frac{\partial\bar{T}}{\partial z}+\Gamma\right)-\frac{1}{2}\frac{\partial\overline{(w'T'^2)}}{\partial z}-\chi, \quad (15)$$

where Γ is the adiabatic lapse rate and χ the temperature variance dissipation. The time rate of change of temperature variance is about two orders of magnitude smaller than the other terms. The dissipation is obtained from the Kolmogoroff hypothesis

$$\theta(k)=\beta\chi\epsilon^{1/3}k^{-5/3}, \quad (16)$$

where the value $\beta=0.31$ was used as suggested by the measurements of Grant *et al.* (1968). It was then necessary to divide the values obtained by this method by two to correspond to the definition of χ given by Grant *et al.* The lapse rate of potential temperature is assumed to be 0.5C km^{-1} for the entire boundary layer; however, the measured lapse rates of Fig. 1 show considerable variation with height. Therefore, the first term on the right cannot be accurately measured, and may, in fact, have the wrong sign at 100 m. The second term is subject to a similar underestimation as the other eddy flux terms. The value of $\overline{(w'T'^2)}$ decreases with height to an almost negligible value at 1000 m. Consequently, the value of $\partial\overline{(w'T'^2)}/\partial z$ in the lowest layer may be too large and in the higher layer too small. The value of β in (10) is not as well established as the corresponding constant for the turbulent kinetic energy dissipation. Consequently, although all the terms in the equation are estimated, and plotted in Fig. 16, the estimates may not be as accurate as the terms in the velocity variance equation.

In contrast to ϵ, the values of temperature variance dissipation decrease markedly with height. The dissipation curve is drawn with a minimum value between 450 and 1000 m height. This is based on the observation that the temperature fluctuations have a minimum value somewhere in this region and then increase somewhat close to the top of the boundary layer, where warmer air from above the inversion is entrained in the boundary layer. In contrast to the velocity spectral densities, which remain almost constant with height, the temperature spectral density decreases by an order of magnitude from 100 to 1000 m above the surface. This is a direct result of the lack of a strong source of temperature variance above the surface layer.

5. Conclusions

The airplane turbulence measuring system described here is capable of measuring vertical air velocity and temperature to wavelengths long enough to measure the vertical flux of sensible heat by the eddy correlation method at 100 m above the surface for strong surface heating and a mean wind of 10 m sec^{-1}. At higher levels the accuracy is degraded because of the longer wavelength limit of significant heat transport.

This wavelength limit is direction sensitive. At 100 m above the surface the crosswind traverses indicate that the thermals are ~200 m across and the traverses parallel to the wind indicate that the thermals are elongated in the direction of the mean wind to greater than 400 m. This directional sensitivity is also evident in the spectral densities of temperature and velocity fluctuations. The spectral densities at the long wavelength end are larger for the traverses parallel to the wind than for those crosswind.

All the terms in the turbulent kinetic energy balance equation except the pressure fluctuation term can be estimated from the airplane data. The kinetic energy dissipation is almost constant with height, while the divergence of the vertical transport of kinetic energy increases with height to balance the decrease in the production of kinetic energy by the buoyancy force. Similarly, the terms in the temperature variance balance equations were evaluated. The temperature variance dissipation as well as the divergence of the vertical transport of temperature variance decrease rapidly with height. In contrast to the turbulent kinetic energy budget, there is no production of temperature variance higher than 100 m in the boundary layer.

APPENDIX

Calculation of Velocity Components

The longitudinal air velocity is obtained from the difference of the Doppler-measured ground speed, GS, and the true airspeed, TAS. The Doppler radar outputs have considerable high-frequency noise and consequently must be smoothed before they can be used. On the other hand, the longitudinal velocity of the airplane does not respond to turbulence at high frequencies. The period of the phugoid oscillation, which is a measure of the longitudinal velocity response time of the airplane, is on the order of 1 min. Taking these factors into account, an averaging time of 10 sec was selected. The longitudinal velocity u_l is given by the sum of the low-frequency variation $\bar{u}_l$ and the high-frequency variation u_l'. Expressed in terms of the ground speed and true airspeed,

$$\left.\begin{aligned} \bar{u}_l &= \overline{\mathrm{GS}} - \overline{\mathrm{TAS}} \\ u_l' &= \overline{\mathrm{TAS}} - \mathrm{TAS} \\ u_l &= \bar{u}_l + u_l' = \overline{\mathrm{GS}} - \mathrm{TAS} \end{aligned}\right\}, \tag{A1}$$

where positive u_l is in the direction of flight.

The vertical velocity is calculated from: 1) the attack angle α which is the angle of the airstream with respect to the airplane in the vertical plane of the airplane; 2) the pitch angle θ which is the attitude angle of the airplane about the lateral axis (obtained by measuring the angle between the gyro-stabilized platform and the airplane); and 3) the vertical velocity of the airplane, which is obtained by integrating the output of a vertically-oriented accelerometer mounted on the stabilized platform. The accelerometer output, $e(t)$, is modified by a low-pass RC circuit with a time constant τ of 3 sec. The output of the filter, $e_0(t)$, is related to the filter input by

$$\tau \frac{de_0}{dt} + e_0 = e. \tag{A2}$$

The airplane vertical velocity is the integrated accelerometer output, which is

$$w_a(t) = \int_0^t e(t)dt + \tau e(t). \tag{A3}$$

Digital integration is performed on the data, recorded at eight samples per second, by Simpson's rule. The resulting finite difference equation is

$$W_a(I) = [E(I-2) + 4E(I-1) + E(I)]/24 + \tau \times [E(I) - E(I-2)] + W_a(I-2). \tag{A4}$$

The advantages of this approach as compared to recording the vertical acceleration directly are that a slower recording rate will yield the same amount of information, and a smaller full-scale recording range is required. At low frequencies, the acceleration is still measured directly so that an accelerometer offset voltage will not drive the output off scale. Combining the variables in the standard equation for calculating the vertical air velocity, we have

$$w = \mathrm{TAS}\sin(\alpha-\theta) - w_a \approx \mathrm{TAS}(\alpha-\theta) - w_a. \tag{A5}$$

The gyro which is used to stabilize the platform is gravity-erected to a nominal earth vertical before each measurement run and then allowed to run free for the duration of the run. The maximum gyro drift rate is 0.0067 deg sec^{-1}, and is very nearly a constant for any given run. This contributes an error of $0.004t^3$ [cm sec^{-1}] (if the platform is initially level) to the measurement of w_a because of the change in magnitude of the measured component of gravitational acceleration. However, the attitude angles and vertical velocity of the airplane are not measured absolutely. The vertical axis of the platform may differ by a degree or more from the local earth vertical. Any accelerometer bias voltage, whether due to initial platform misalignment, changes in the magnitude of the gravitational acceleration, or changes in the electronic circuitry, will result in an error in w_a proportional to time; any linear drift in the accelerometer output will result in an error proportional to time squared. Therefore, a least-squares fit with a second-order polynomial, $(a_0 + a_1 t + a_2 t^2)$, is made to the vertical air velocity for each measurement run.

The lateral air velocity is calculated from: 1) the sideslip angle β, which is the angle of the airstream with respect to the airplane in the horizontal plane of the airplane; 2) the yaw angle ψ, which is the instantaneous aircraft heading minus the average heading over the particular run (measured with a gyro-stabilized magnetic compass); 3) the airplane drift angle δ, which is the angle between the airplane and its flight path (measured with the Doppler radar); and 4) the ground speed and the true airspeed. The angles increase in value when rotated clockwise about the z axis (pointing up). The lateral air velocity with respect to the average aircraft heading is given by

$$v_l = \overline{\mathrm{GS}\sin(\delta-\psi)} - \mathrm{TAS}\sin(\beta-\psi), \tag{A6}$$

where the bar again indicates an average over 10 sec. The lateral air velocity is positive when the air is moving from left to right across the front of the aircraft. Again, it is assumed that the velocity of the airplane with respect to the earth does not change significantly in that time.

Acknowledgments. I gratefully acknowledge the assistance of K. Danninger and W. Glaser in the development of the aircraft instrumentation, and R. Lackman in programming and processing the data tapes. I am indebted to the NCAR Aviation Facility for providing the airplane, the recording system, and additional instrumentation. I also thank J. Deardorff and D. Lilly for offering many helpful suggestions that have been incorporated in this paper.

REFERENCES

Businger, J. A., and J. W. Deardorff, 1968: On the distinction between "total" heat flux and eddy heat flux. *J. Atmos. Sci.*, **25**, 521–522.

Deardorff, J. W., 1970: A three-dimensional numerical investigation of the idealized planetary boundary layer. *Geophys. Fluid Dyn.*, **1**, No. 3 (in press).

Gossard, E. E., 1960: Spectra of atmospheric scalars. *J. Geophys. Res.*, **65**, 3339–3351.

Grant, H. L., B. A. Hughes, W. M. Vogel and A. Moilliet, 1968: The spectrum of temperature fluctuations in turbulent flow. *J. Fluid Mech.*, **34**, 423–442.

Hardy, K. R., and H. Ottersten, 1969: Radar investigation of convective patterns in the clear atmosphere. *J. Atmos. Sci.*, **26**, 666–672.

Holloway, J. L., Jr., 1958: Smoothing and filtering of time series and space fields. *Advances in Geophysics*, Vol. 4, New York, Academic Press, 351–389.

Kaimal, J. C., and J. A. Businger, 1970: Case studies of a convective plume and a dust devil. *J. Appl. Meteor.*, **9**, 612–620.

Keuttner, J., 1959: The band structure of the atmosphere. *Tellus*, **11**, 267–294.

Myrup, L. O., 1969: Turbulence spectra in stable and convective layers in the free atmosphere. *Tellus*, **21**, 341–354.

Panofsky, H. A., and E. Mares, 1968: Recent measurements of cospectra for heat-flux and stress. *Quart. J. Roy. Meteor. Soc.*, **94**, 581–585.

——, and F. Pasquill, 1963: The constant of the Kolmogoroff law. *Quart. J. Roy. Meteor. Soc.*, **89**, 550–551.

Sasamori, T., 1968: The radiative cooling calculation for application to general circulation experiments. *J. Appl. Meteor.*, **7**, 721–729.

Warner, J., and J. W. Telford, 1962: On the measurement from an aircraft of buoyancy and vertical air velocity in cloud. *J. Atmos. Sci.*, **19**, 415–423.

——, and ——, 1963: Some patterns of convection in the lower atmosphere, *J. Atmos. Sci.* **20**, 313–318.

——, and ——, 1965: A check of aircraft measurements of vertical heat flow. *J. Atmos. Sci.*, **22**, 463–465.

Woodcock, A. H., 1942: Soaring over the open sea. *The Scientific Monthly*, **55**, 226–232.